

MODELLING TURBULENT FLOW WITHIN NUCLEAR HEAT EXCHANGERS

H. IACOVIDES^{*}, B.E. LAUNDER^{*} AND A. WEST^{*†},

^{*} Turbulence Mechanics Group, School of MACE, University of Manchester, M60 1QD, UK,
hector.iacovides@manchester.ac.uk, brian.launder@manchester.ac.uk, www.manchester.ac.uk

[†] CD-adapco, 200 Shepherds Bush Road, London, W6 7NL, UK,
alastair.west@cd-adapco.com, www.cd-adapco.com

Key Words: *In-line tube banks, Convective heat transfer, Heat exchangers, URANS, LES.*

Abstract. This paper reports experiences from applying Large Eddy Simulation (LES) and Unsteady Reynolds-Averaged Navier Stokes (URANS) approaches for modelling turbulent flow and heat transfer around in-line tube banks. The important effect of confining walls has been examined, firstly, by making direct comparisons with the square in-line 4×7 tube bank of Aiba et al. [1]. Finally, a specific design of in-line tube bank used within Advanced Gas-cooled Reactors (AGR) [2] is simulated using the URANS approach.

1 INTRODUCTION

Engineering applications of cross-flow tube banks are abundant. Such configurations achieve high heat transfer with relatively low manufacturing complexity, making them attractive heat exchangers for use in fossil-fuel and nuclear power plants. Reliable prediction of the flow and heat-transfer characteristics of such tube-bank flows is therefore essential for heat-exchanger design and life-time management. Such heat exchangers may consist of arrays of hundreds or even thousands of tubes, through which a fluid passes while a second fluid is blown normal to them, the overall purpose being to promote heat exchange between the two fluids. Detailed testing on such systems, both experimental and computational, is largely done on much smaller systems, typically consisting of clusters from four to a few tens of tubes, the hope being that the data emerging will be representative of those in the full-scale plant.

Experiments on widely-spaced in-line and staggered tube banks have been carried out inter alia by Ishigai et al. [3] where several distinct flow patterns were observed. Costs with tightly packed bundles are lower, however, and extensive data have been reported on close-packed staggered tube banks. There are few experiments of closely-spaced in-line tube banks and even fewer providing data of local heat transfer [1].

Large-eddy simulations (LES) and Unsteady Reynolds-Averaged Navier Stokes (URANS) simulations of closely-spaced square in-line tube banks have been performed recently by the authors (West [4], Iacovides et al.[5]). The assumption of flow periodicity in all three directions was investigated by varying the domain size. It was found that the path taken by the fluid through the tube bank configuration differed according to the assumed flow

dimensionality (2- or 3-dimensional), the pitch-to-diameter ratio, P/D , and the treatment of turbulence. As the pitch:diameter ratio decreased the flow deviated from the symmetric flow patterns observed by Ishigai et al. [3], the mean flow preferring to travel in a diagonal path through the domain. Such a flow path has seldom been seen in experiments in such small arrays because then the confining wind-tunnel walls restrict cross-flow motion. However, Aiba et al. [1] noted, for $P/D=1.2$ with only 4 tubes in the cross-flow direction, that “it is very clear that the flow through the tube bank deflects as a whole”. Jones et al. [2] also reported cross-flow drift in their 22×22 tube test section, which was representative of the in-line section of an AGR heat exchanger, see Figure 1. Several internal documents [6,7] report this particular configuration to have good thermal mixing properties where temperature spikes that were inserted into the inlet were seen to ‘drift sideways’ as they propagated through the bank. This 3-dimensional, large-scale, convective secondary motion is very significant compared to the turbulent eddy motions. Thus, if one is seeking to model the flow through the bank using a 2-dimensional lumped-parameter code, it is essential to prescribe an enhanced lateral thermal diffusivity to account for this augmented transport.

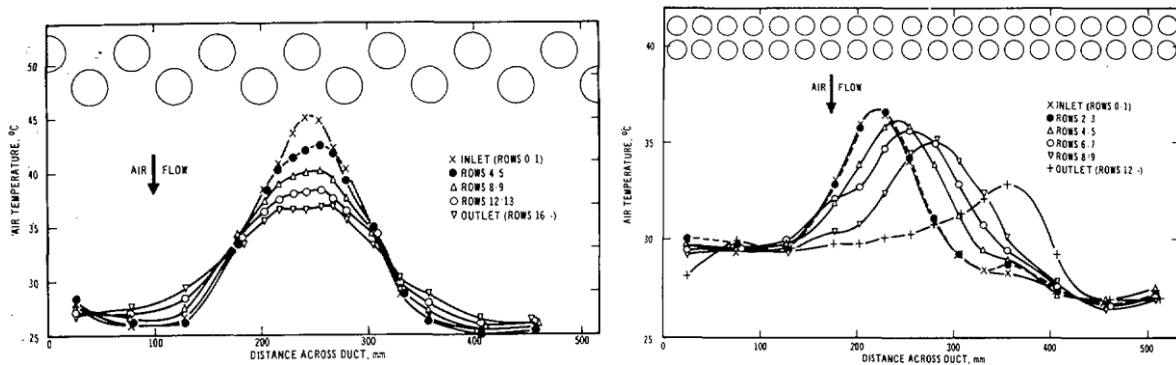


Figure 1: Measurement of a hot temperature spikes through a staggered (left) and in-line (right) tube bank. Taken from Jones et al. [2].

The present paper focuses on the effects of confining walls via three-dimensional URANS and LES modelling by making direct comparison with the limited experimental data available. Firstly, the generic, square, in-line 4×7 tube bank is examined corresponding to the experimental data of Aiba et al. [1]. Secondly, a specific in-line 10×12 tube bank found within an AGR heat exchanger is examined corresponding to the experiment of Jones et al. [2]. The pitch-to-diameter ratio of the former bank is 1.6 square (meaning both longitudinal and transverse pitches are equal). In contrast, the industrial tube bank [2] has an alternating longitudinal pitch-to-diameter ratio of 1.33 and 2.0 and a transverse P/D of 1.39. As there are very limited data concerning the latter industrial bank (mainly comprising just a number of temperature profiles across the bank) the present enquiry is focused on gaining an appreciation of the flow behaviour.

2 COMPUTATIONAL AND PHYSICAL MODELS

2.1 Computational Domain

It is not currently practicable, still less economic, to compute in detail a complete tube-bank assembly as used in industry. Nevertheless, the relatively small configurations employed by Aiba et al.[1] and Jones et al. [2] can, at least with a URANS treatment, be computed in their entirety to allow a more precise comparison with experiment. The former configuration is used to judge the relative accuracy achieved by the different turbulence modelling approaches. This complete flow configuration appears in Fig. 2(a), which was mapped with 23 and 41 million cells for the high-Re and low-Re meshes respectively. For an LES treatment, the considerable computational resource only enabled the simulation of a 4×4 array with the important addition that, while repeating boundaries were placed in the streamwise and spanwise directions, Fig 2(b), a fine mesh was adopted approaching the upper and lower wall surfaces which were thus fully resolved. This LES mesh amounted to 12 million cells. A block-structured hexahedral topology gave greater control of the number of cells and a more effective resolution of the near-wall regions.

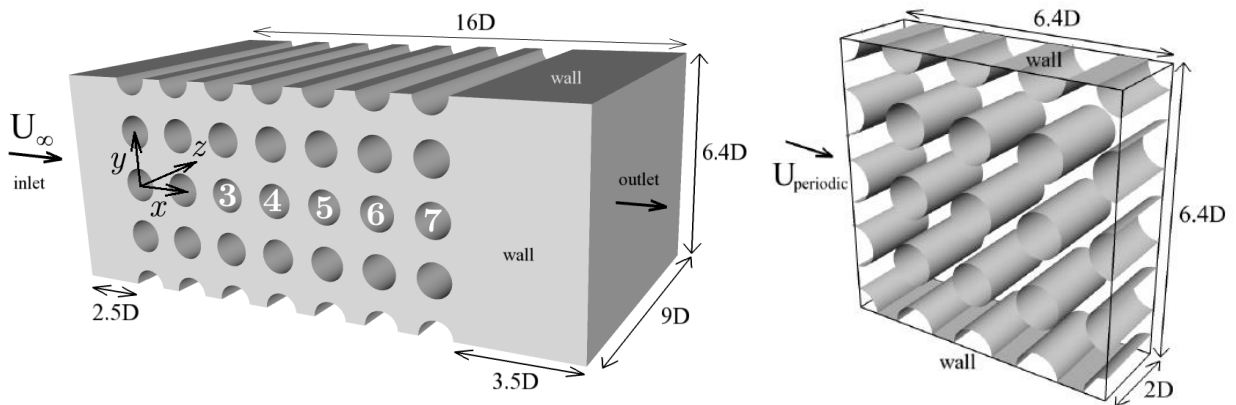


Figure 2: Flow coverage for the configuration of Aiba et al. [1] (a) URANS (b) LES

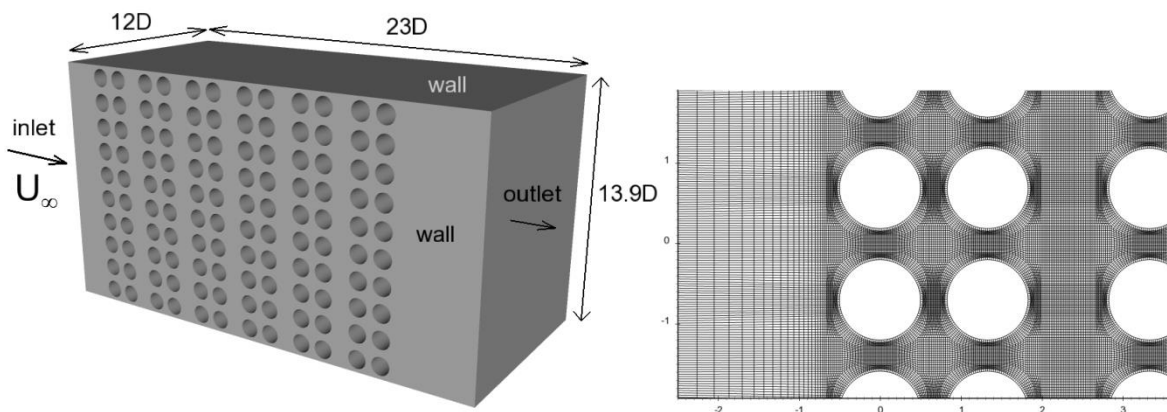


Figure 3: (a) Flow coverage for the configuration of Jones et al. [2] (b) Close-up of high-Re URANS mesh

Because Jones et al. [2] tracked the diffusion of temperature spikes through the bank, the heat transfer to the tubes is no longer significant so the rudimentary wall functions incorporated within the software adopted could be used to keep computational expenses relatively low. Nevertheless, this still resulted in a mesh size of 42 million cells for the case at a Reynolds number of 66,000. A preliminarily fully-periodic 2×2 tube section was simulated with both LES and URANS (SSG model with wall functions) which broadly validated the use of URANS approach, giving similar cross-flow velocities, see West [4] for more details.

2.2 Discretization Practices and Boundary Conditions

Both LES and URANS approaches have employed the finite-volume code, *Code_Saturne* [8] with a collocated grid. It was decided to use this freely available and versatile software although it does not offer some of the more advanced modelling practices incorporated in our in-house code, STREAM [9]. However, a few computations were also made with the latter code [4] which broadly confirmed the conclusions reached with *Code_Saturne*. The velocity-pressure coupling is achieved by a predictor/corrector method using the SIMPLEC algorithm where the momentum equations are solved sequentially. The Poisson equation for the pressure field is solved using a conjugate-gradient method and a standard pressure-gradient interpolation to avoid oscillations. As spatial and temporal discretisation are second order (central-difference and Crank-Nicolson interpolations respectively), the time step was kept sufficiently small to ensure the maximum Courant number was below unity.

Where possible experimental conditions are replicated, resulting in Reynolds numbers of 41,000 and 66,000 based on the tube diameter, D , the kinematic viscosity of the fluid, ν and the bulk gap velocity, U_g for the generic and industrial tube banks respectively. A 3% and 5% turbulent intensity were used at each inlet for the generic and industrial tube banks respectively. A uniform heat flux is prescribed on the tube surfaces for the generic tube bank. For the LES flow periodicity is used, a constant mass flow rate is imposed to obtain the desired bulk velocity by specifying an explicit self-correcting mean pressure gradient at every time step. Thermo-physical fluid properties are assumed to be constant.

For the URANS computations, grid-sensitivity studies were first performed for both high-Re (i.e. used with wall functions) and low-Re (integration to the wall) grids (details of these studies are given in West [4]). A factor of 1.1 is used for the radial cell-expansion from the tube walls and 160 cells were used around the tube surface. The centre of the wall-adjacent cell is located at $y^+ = \Delta y^+ / 2 \approx 0.25$ over most of the cylinder wall. The spanwise resolution is chosen in order that in the central region cell dimensions were comparable with those in the streamwise and cross-wise direction (i.e. they were as close as possible to a regular hexahedron or a cube). This resulted in wall units of $\Delta x^+ < 60$ and $\Delta z^+ < 80$ over the wall surfaces. A detailed LES domain size and grid dependency study was conducted on a fully-periodic configuration reported in Iacovides et al. [5] where doubling the spanwise resolution (z direction) had little effect on the overall flow pattern.

The larger industrial configuration of Jones et al. [2] followed a similar mesh resolution as that of the generic configuration, Figure 3b, only fewer cells were possible in the spanwise, z , direction, resulting in only 6 cells per diameter.

2.3 Turbulence Modelling

The turbulence models used for the URANS calculations are both Reynolds Stress Models (RSMs), that is, models where individual transport equations are solved for each of the Reynolds stresses. In principle such models should have significantly wider applicability than eddy viscosity models, albeit at typically twice the computational cost. A key requirement in modelling at this level is properly accounting for the damping of turbulence caused by the complex arrangement of solid surfaces. Both models considered can be said to be (substantial) developments from the early model of Launder et al. [10]. That scheme introduced damping functions into the key pressure-strain process whose magnitude depended on the ratio of the local turbulent length scale to the distance of a point from the wall, a strategy that seemed acceptable for the flat surfaces originally considered. That arrangement would be unworkable in a tube bank, however. The so-called ‘elliptic-blending’ model of Manceau & Hanjalić [11] provides the wall-proximity damping by applying an elliptic-relaxation strategy and uses a slightly simplified form of the SSG model for the ‘homogeneous’ part of their pressure-strain model which becomes dominant well away from the tubes. The SSG model proposed by Speziale et al. [12] avoids the need for particular wall-damping corrections by the choice of models for the different parts of the pressure-strain model. However, the model cannot cope with the extreme anisotropy of the stresses in the ‘buffer’ region very close to the wall and thus must be used with the ‘scalable’ wall functions of [13].

The extra information provided by the values of all the Reynolds stresses (rather than just the turbulent kinetic energy) enables a more general, though still very simple, model to be used for computing turbulent heat fluxes, namely the generalized gradient-diffusion hypothesis. Further details of each model can be found in the respective references.

The wall-resolved LES uses the dynamic Smagorinsky model [14] and least squares minimisation of Lilly [15] to model the sub-grid-scale stress tensor. The current LES procedure is the same as that used by Kahil [16] in his study of flow over single and tandem cylinders. The Smagorinsky coefficient was limited between 0 and 0.065 and 1% local blending with upwind was used to avoid artificial numerical oscillations with 2nd-order central differencing. As heat-transfer predictions were a major practical output for the Aiba test case, the immediate near wall region was resolved via a fine mesh rather than sgs wall functions.

3 COMPUTATIONAL RESULTS

3.1 Square In-line Tube Bank

The inclusion of walls (compared with the repeating boundaries of [5]) naturally removed the possibility of the flow taking a skewed path through the tube bank and it is seen in Fig. 4a that the computed pressure coefficient is, in consequence, symmetric about the horizontal centreline through the cylinder. The agreement of the LES computations with the measurements by Aiba et al. around the 6th cylinder in their array is close. The corresponding Nusselt number distributions around the tube appear in Fig. 4b. The peak Nusselt number occurs for $\theta=45^\circ$; that is, close to, but not precisely coincident with, the stagnation point. The experimental data around the 6th tube show approximately the same position of maximum Nusselt number but in general less variation in magnitude around the cylinder than the LES

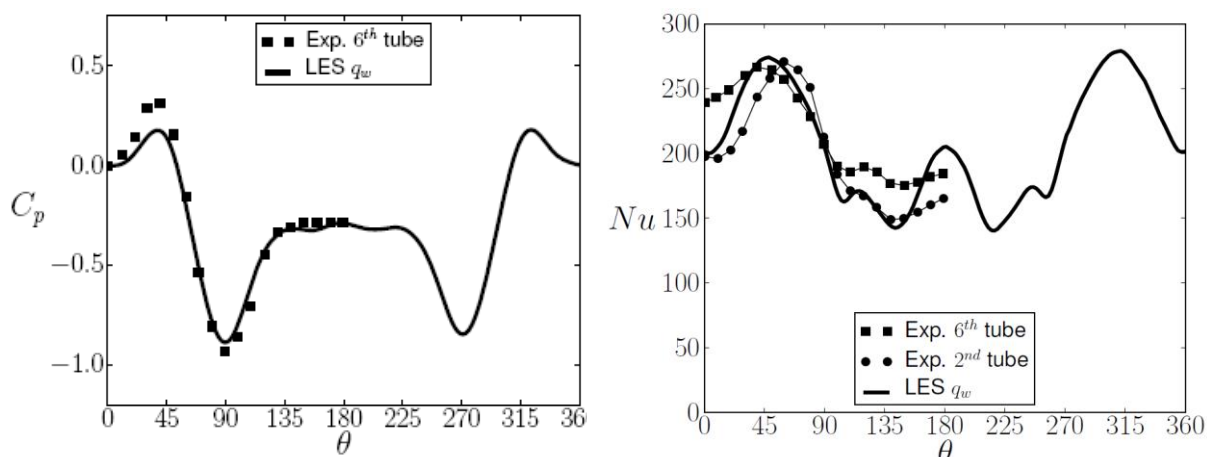


Figure 4: LES Spanwise-averaged Pressure Coefficient (left) and Nusselt number distribution (right).

result. Part of this difference could arise from internal conduction within the heater foil. That is, since a uniform heat flux is applied via an electrically heated foil, the very front of the cylinder will be hotter than at the position of maximum Nu . There will thus be a tendency for some of the heat generated by the foil heater to be conducted around to the cooler part of the cylinder leading to a smaller indicated circumferential variation of Nu than would actually pertain. An unavoidable difference between the LES and experiment is that the LES computations adopt fully-developed boundary conditions whereas the experiment heated just one cylinder. While the LES values of Nu are based on the bulk temperature just ahead of each cylinder, because there is a small vertical variation of temperature in the fluid, the two Nusselt numbers are not precisely equivalent. Both of these effects would tend to bring the LES and experimental data into closer agreement though our best, albeit imprecise, estimates are that together they are not large enough to account completely for the differences shown in Fig. 4. (It is noted that an earlier experiment by the same authors, Aiba et al. [17], of a single row of four in-line cylinders compared Nusselt numbers measured by heating a single cylinder, as above, with those obtained from heating all tubes. For the third cylinder, the mean Nusselt number with all tubes heated was less than 5% below that for the case where just the third cylinder was heated).

In Fig. 6 the variation of mean and rms turbulent streamwise velocities along a line midway between cylinders is compared with the experimental data measured mid-way between the 4th and 5th row, i.e. as far downstream as possible without risking significant exit effects (there being 7 rows of tubes). Two things should be noted: firstly that, while the maximum velocity agrees very closely with experiment, the LES gives a reverse flow region directly behind the tubes that is entirely missed by the experiments. (However, in displaying the LES mean velocities, the reverse flow region has been ‘flipped’ to positive. This change of sign accords with the constraints arising from the experimental velocity field data which had been measured with a hot-wire anemometer, an instrument incapable of recording back-flow unless used in ‘flying-hot-wire’ mode, which was not the case here). Moreover, the turbulence data obtained in this way would also record levels of turbulence that were much too low. The presence of the recirculating region behind each cylinder row (shown more clearly in the LES mean streamline plot of Fig. 5) is clearly inferable from the pressure

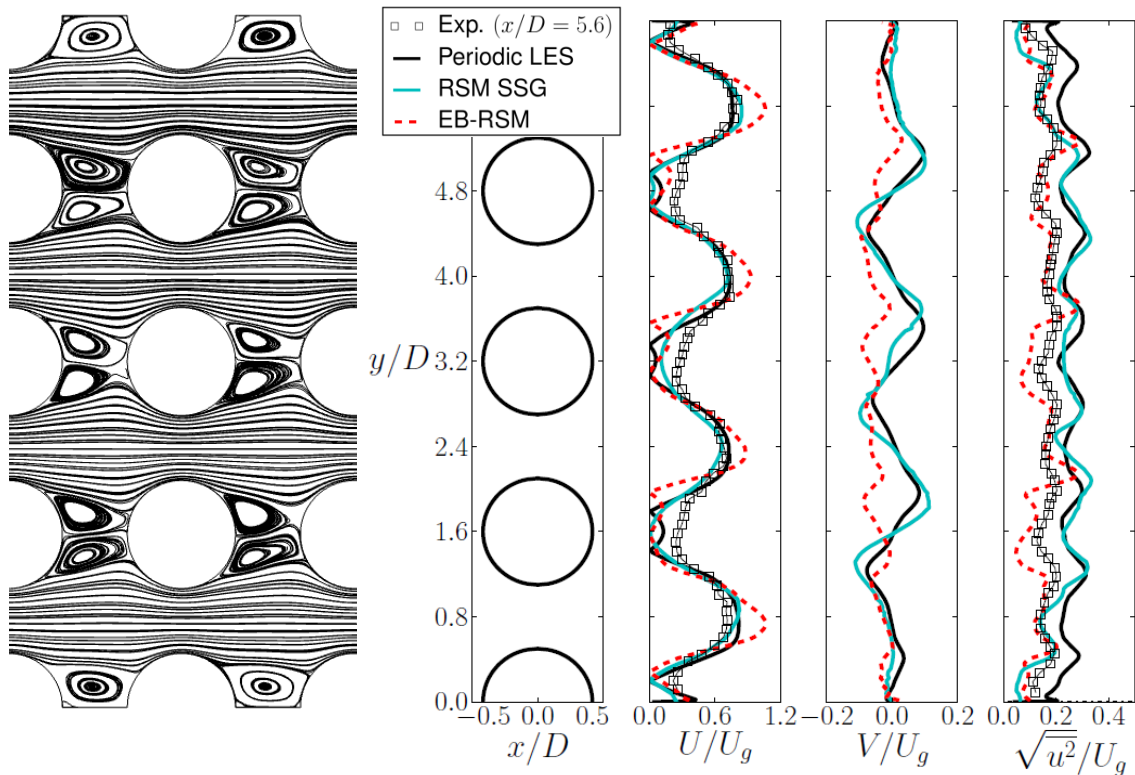


Figure 5: Mean streamlines for LES (left) and mean and rms streamwise turbulent velocities.

distribution in Fig. 4 which shows a pressure maximum in both the experiment and the computations at $\theta=40^\circ$, a feature signalling the presence of a stagnation point on the cylinder at that location. Evidently, the velocity measurements failed to capture the sequentially reversing, high-intensity turbulent flow in that region. The second point to note is that a second LES computation was run with only two complete rows in the stream direction. There are small but detectable differences in the mean velocity profile in the centre region and somewhat larger effects on the turbulence intensity indicating that the large-scale turbulence structures are not fully captured with a domain length of two diameters. Interestingly, the differences reduce as one proceeds closer to the upper and lower confining walls, indicating that the walls are exerting some effect in limiting the length scale. (The reason that the computations of flow through the quasi-infinite tube bank in Iacovides et al [5] showed no significant difference between the 2×2 and 4×4 computations was presumably that, for this case, the flow adopts a diagonal passage through the bank creating lower and finer scale turbulence that requires a shorter distance over which to be resolved.)

In considering the different aspects of the URANS performance, West [4] examined both 2- and 3-dimensional flows. Here attention is limited just to the 3-dimensional case since only these computations take account of the impact of all the containing walls. Moreover, practical constraints such as the project's computational budget, have meant that it was only feasible to explore a small subset of models in this 3-dimensional mode. We thus chose to examine the two second-moment closures since this is a higher-order closure level that might provide an exemplar of what is currently achievable at the URANS level. All the URANS models run in 3D predict a periodic, vortex shedding behaviour, as seen from Figure 6 which compares the

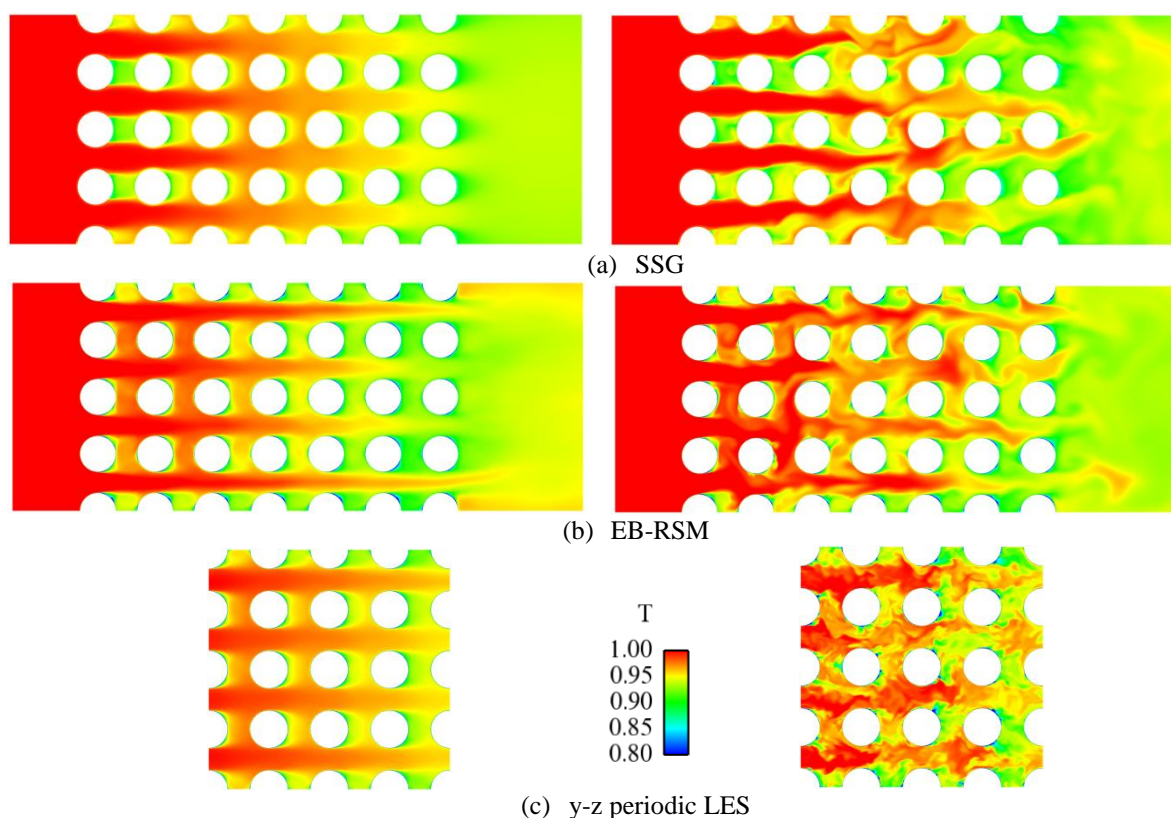
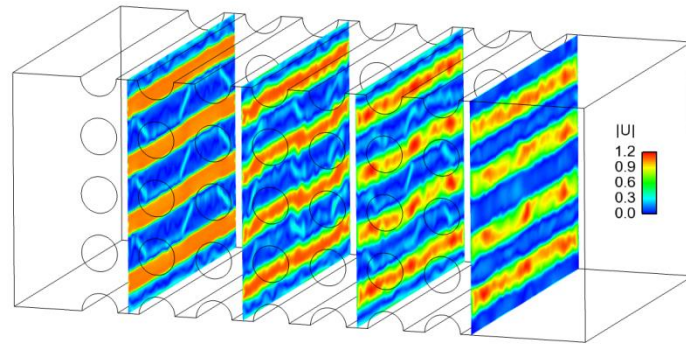


Figure 6: Spanwise-averaged (left) and instantaneous (right) temperature field.

long-time averaged thermal field with the instantaneous one.

Figure 5 also compares the inter-row mean velocity and turbulence intensity profiles generated by the different approaches (with again the reverse-flow region found especially with the EB-RSM model flipped to positive). Agreement between the SSG and the formerly presented LES results is close while the EB-RSM profiles suggest that insufficient mixing has occurred in the outer region. While the streamwise turbulence intensity for the EB-RSM is in reasonably close accord with the data of Aiba et al. [1] – certainly closer than the LES/SSG results – it was noted above that the use of a hot-wire anemometer would give serious errors in mean velocity in regions where the velocity direction was reversing and, thus, appreciably too low levels of turbulence.

One of the most interesting features to emerge from these complete-configuration results was the extent to which the enclosing walls altered the structure of the flow as a whole. Figure 7 shows contours of the streamwise (U) and vertical (V) mean velocities midway between the 1st and 2nd rows (Plane 1), 3rd and 4th rows (Plane 3) and the 5th and 6th rows (Plane 5) for the EB-RSM predictions (though broadly similar results were returned with the SSG scheme). Notice that the positions in the cross-section where the V velocity is positive on Plane 3 correspond with regions of negative V on Plane 5 and vice versa. A consequence of this secondary flow is the corresponding difference in the U contours on the two planes. A further consequence is that the distribution of Nusselt number around the cylinder at any point is no longer symmetric about the horizontal bisector through the cylinder centre. Figure 8 shows



Location of planes 1, 3, 5 and 7

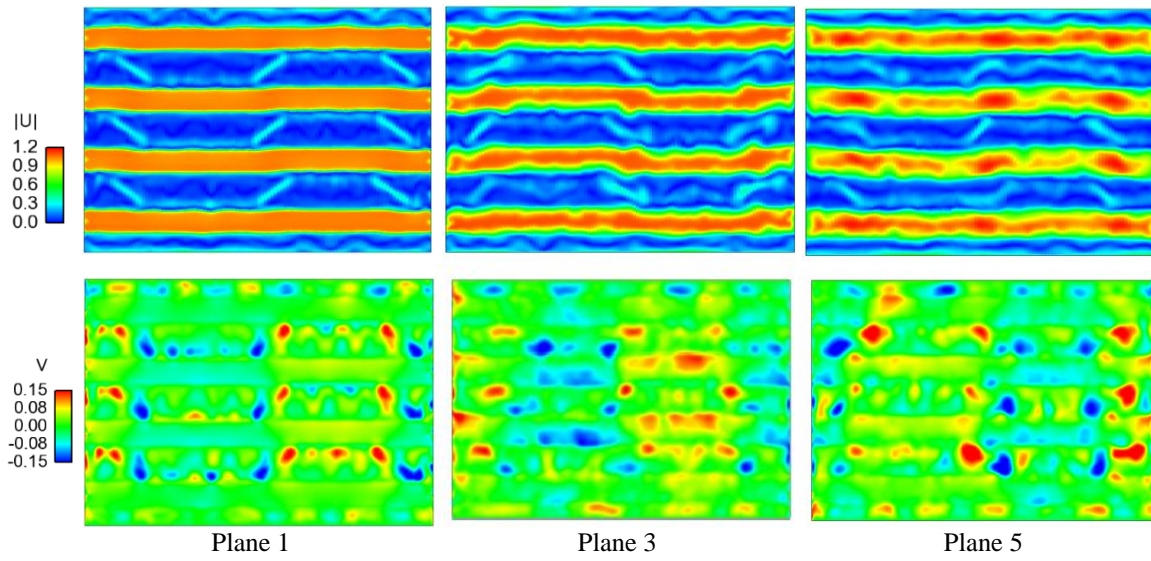


Figure 7: Mean streamwise (top) and crossflow (bottom) velocity components at different planes.

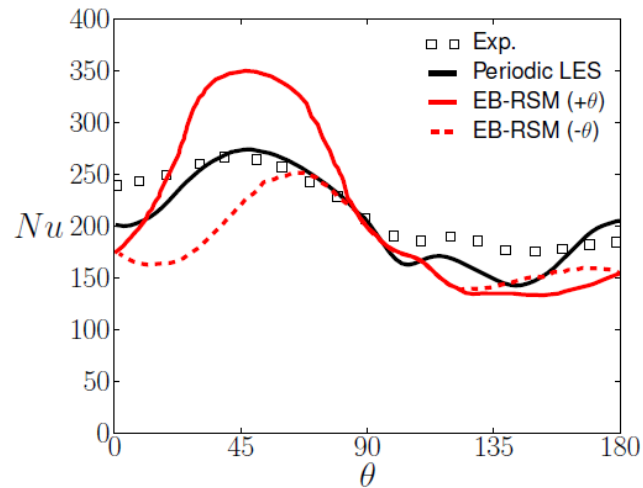


Figure 8: Nusselt number distribution around the centre of the 6th tube in the generic tube bank. Continuous and solid lines indicate the variation around the upper and lower halves of the cylinder using the EB-RSM.

the variation of Nu around the 6th tube compared with the experimental and LES results. One notes that the EB-RSM results exhibit substantially different variations of Nu over the upper and lower surfaces for the leading 70° of arc. If, however, these two values are averaged, reasonably close agreement is achieved with both the LES and the experimental data.

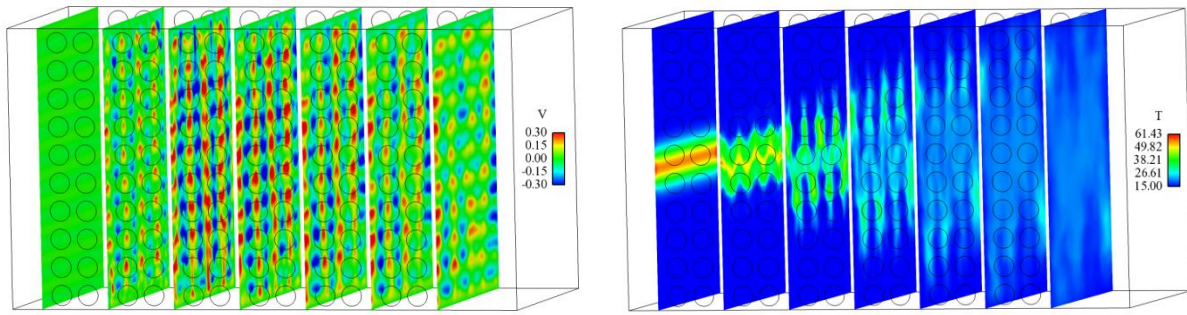
3.2 Industrial In-line Tube Bank

Once the small-scale turbulent fluctuations associated with the periodic vortex shedding are averaged for a long-time period, stable large-scale secondary vortices are predicted. The extent of this can be seen in Figure 9 where the mean cross-flow velocities are shown at different planes through the tube bank. A 2-dimensional Gaussian temperature spike was inserted at the inlet to replicate the experimental technique used to assess the thermal diffusivity of a bank, Figure 9. Clear drifting of the temperature spike is seen upward and downward depending on the flow path, which broadly confirms the findings of Jones et al [2], Tan [6] and Madan [7]. The downstream evolution of mean temperature profiles are plotted alongside that of Madan [7] at one particular span-wise location of $z/D=3$, Figure 10. Note the change of flow orientation to a downward direction and also the change of scale in the y axis to reflect the 22 tubes Madan used in the cross-flow direction. It is clear from Figure 10 that further lateral movement of the temperature spike is prevented by the confining wall which is not the case for the geometry of Madan. This particular span-wise location showed the URANS approach to predict larger diffusive mixing compared to that of the experiments; however, other span-wise locations showed the opposite to occur. West [4] provides details of how these decaying temperature profiles were fitted to analytical temperature profiles in order to quantify the levels of thermal diffusion within the bank. This data ultimately confirmed the high thermal mixing coefficient used by the 2-dimensional lumped-parameter code to predict current operating conditions.

12 CONCLUSIONS

In modelling the complete (but small) tube-bank examined experimentally by Aiba et al [1] the URANS second-moment closure results suggest that significant secondary flows are created within the tube assembly with the flow deflection alternating along the length of any (horizontal) tube between upflow and downflow and with the sense of deflection reversing with distance downstream every two rows. Despite the lack of symmetry arising from these secondary motions, the second-moment closure of Manceau & Hanjalić [11] returned satisfactory predictions of the Nusselt number distribution around the cylinder when averaged around the upper and lower halves. This result clearly underlined the merits of integration to the wall or at least of avoiding overly simplistic wall functions to characterize the near-wall mixing. However, further from the wall (as evidenced by the mean and turbulence velocity profiles) the mixing processes are better reproduced by the SSG second-moment closure of Speziale et al [12]. Since the ‘homogeneous’ part of the EB-RSM model is nearly the same as the SSG model it could be that the elliptic-relaxation component of the former is having an adverse effect despite its evident success within the viscosity-affected sublayer.

Somewhat more pronounced secondary flows are predicted in modelling the industrial tube-bank of Jones et al. [2]. Of the few comparisons that can be made, the levels of thermal diffusivity obtained from the decay of the 2D Gaussian profile inserted at the inlet, show



Location of planes 1, 3, 5 and 7

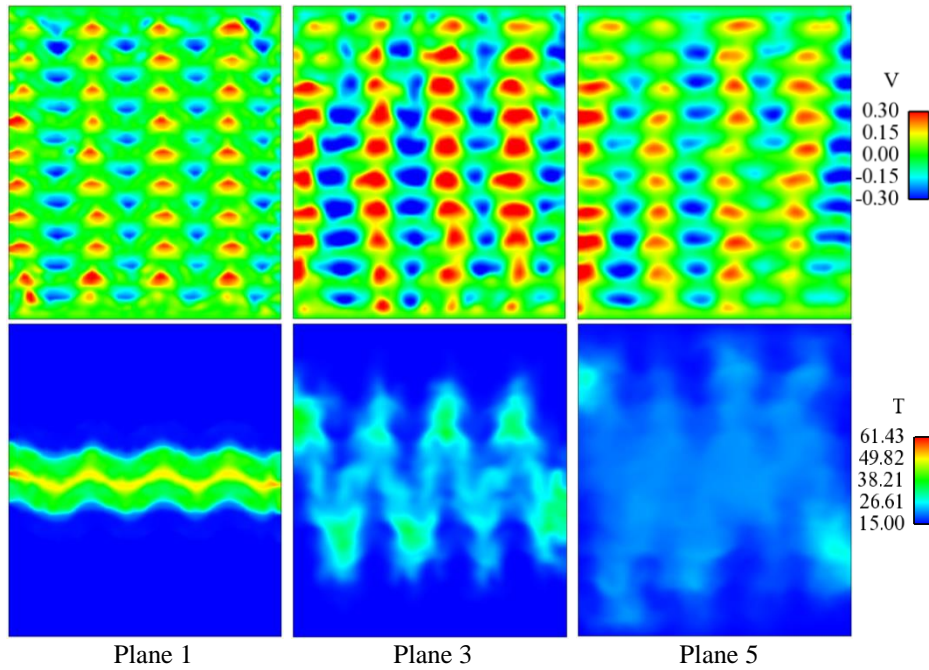


Figure 9: Mean cross-flow velocity (top) and mean temperature field (bottom) at different planes.

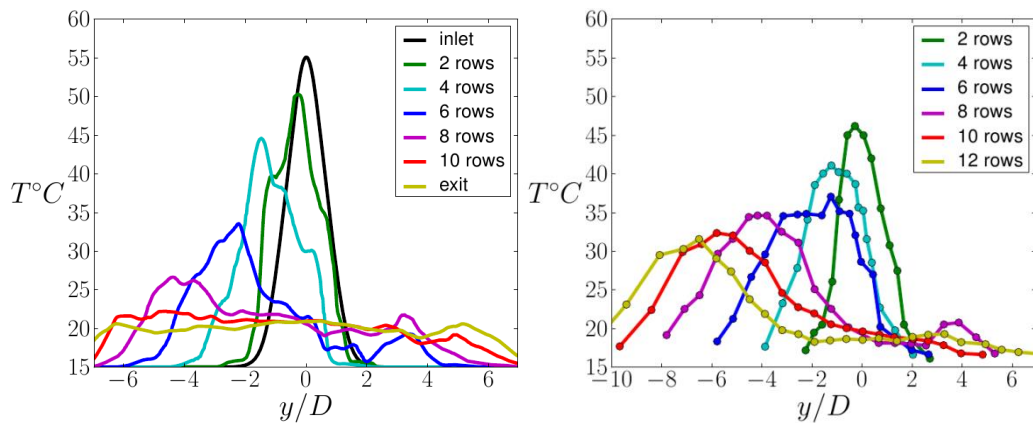


Figure 10: Mean temperature profiles of URANS (left) and from Madan [6] (left) at same spanwise distance but different downstream locations.

reasonable agreement with the experiments.

ACKNOWLEDGEMENTS

The computational support provided by the Barcelona Supercomputing Centre, funded by the HPC Europa-2 Scheme and the EPSRC's UK national high-performance computing facility, HECToR (high-end computing terascale resource), is gratefully acknowledged. The research was supported through the EPSRC doctoral training grant EP/G037426/1 with complementary support from British Energy Generation (now EDF Energy). The authors gratefully acknowledge the help and support of Professor D. Laurence. The active participation and support of EDF Energy staff is warmly acknowledged.

Authors' names are sequenced alphabetically.

REFERENCES

- [1] Aiba, S., Tsuchida, H. and Ota., T. 1982, Heat transfer around tubes in in-line tube banks. *Bull. JSME* **25** (204), 219–926.
- [2] Jones, R., J. Lis, and T. Massey. 1978, An experimental investigation of thermal mixing in crossflow tube banks. In *Proc. of 6th Int. Heat Transfer Conf.*, Paper HX12, Toronto.
- [3] Ishigai, S., Nishikawa, E. and Yayi, E. 1973, Structure of gas flow and vibration in tube banks with tube axes normal to flow, *Proc. Int. Symp. on Marine Eng.*, Tokyo, Japan, 1-5-2-1-15-33.
- [4] West, A., 2012, Assessment of computational strategies for modelling in-line tube banks, *Eng. Thesis*, The University of Manchester.
- [5] Iacovides, H., Launder, B.E. and West, A. 2013, Alternative strategies for modelling flow over in-line tube banks. *Proc. 8th Int. Symp. Turb. Shear Flow Phenomena*, Poitiers, France.
- [6] Tan, R.H. 1981, Heyshem II and Torness development: Boilers. Investigations into in-bank gas mixing of the evaporator/primary superheater sections. Technical Report RD/P/998.
- [7] Madan, V.K. 1981, Investigations into gas mixing in future AGR boilers. Technical Report RD/P/993, PERSC.
- [8] Archambeau, F., Mechtoua, N. and Sakiz, M., 2004, Code Saturne: a finite volume code for the computation of turbulent incompressible flows, *Int. J. Finite Volumes, Industrial Apps*, 1, 1-62.
- [9] Lien, F-S and Leschziner, M. A. 1994, A general non-orthogonal finite-volume algorithm for turbulent flow at all speeds incorporating second-moment closure, *Comp. Meth Appl. Mech Eng*, 114, 123-167.
- [10] Launder, B.E, Reece, G.J. and Rodi, W. 1974. Progress in the development of a Reynolds-stress turbulence closure, *J. Fluid Mech.* **68**(3), 537-566.
- [11] Manceau, R. and Hanjalić, K. 2002, Elliptic blending model: A new near-wall Reynolds-stress turbulence closure, *Phys. Fluids* **14** (2), 744–754.
- [12] Speziale, C. G., Sarkar, S. and Gatski, T. B., 1991, Modelling the pressure-strain correlation of turbulence: an invariant dynamical systems approach. *J. Fluid Mech.* **227**, 245–272.
- [13] Grotjans, H. and Menter F., 1998, Wall functions for general application CFD codes, in *Proc 4th European Comp. Fluid Dyn. Conf.*, Athens, Greece, 1112–1117.
- [14] Germano, M., Piomelli, U., Moin, P. and Cabot, W.H. 1991. A dynamic subgrid-scale eddy viscosity model. *Physics of Fluids A: Fluid Dynamics* **3**(7), 1760-1765.
- [15] Lilly, D. K., 1992, A proposed modification of the Germano sub-grid-scale closure method, *Phys. Fluids A: Fluid Dynamics* **4**, 633–635.
- [16] Kahil, Y., 2011, Simulation des grandes échelles d'écoulements turbulents autour de cylindres circulaires à un nombre de Reynolds sous critique, *PhD Thesis*, Institut d'Alembert, Université Pierre et Marie Curie, Paris, France.
- [17] Aiba, S., Tsuchida, H. and Ota, T., 1981, Heat transfer around a tube in a bank, *Bull. JSME* **24** (188), 380-387.